RSC Advances

ROYAL SOCIETY OF CHEMISTRY

www.rsc.org/advances

A six-metal $\{Na_2Cu^{I}Cu^{II}_3\}$ sandwich-type heteropolyanion shows excellent catalytic activity for electron transfer reaction of ferricyanide to ferrocyanide by thiosulphate.

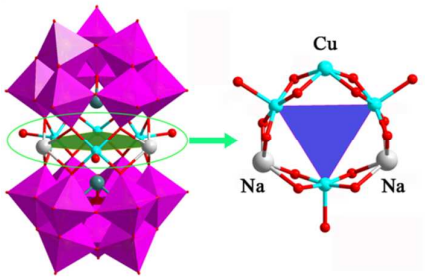

Journal Name

RSCPublishing

ARTICLE

Synthesis of a Novel Cu^{I}/Cu^{II}-containing Sandwich-type Cluster and Its Catalytic Electron Transfer Property

Cite this: DOI: 10.1039/x0xx00000x

Received 00th January 2012,
Accepted 00th January 2012

DOI: 10.1039/x0xx00000x

www.rsc.org/

Xiaolong Xue,[a] Xiaofang Zhao,[a] Deshun Zhang,[a] Zhangang Han,[a,]* Haitao Yu,[a] and Xueliang Zhai [a,]*

A novel six-metal sandwich-type heteropolyanion $[Na_2Cu^{I}Cu^{II}(OH_2)Cu^{II}_2(B\text{-}\alpha\text{-}SbW_9O_{33})_2]^{9-}$ (**1**) has been synthesized in good yield from a one-pot hydrothermal reaction and characterized by IR, XPS, XRD and TG. Single-crystal X-ray analysis reveals that compound $H_9[Na_2Cu^{I}Cu^{II}(OH_2)Cu^{II}_2(B\text{-}\alpha\text{-}SbW_9O_{33})_2]\cdot 9H_2O$ (**H_9-1**) crystallizes in tetragonal system with space group of $P\text{-}42_1m$, and consists of a 2D inorganic network based on Cu-O-W linkages among polyanionic clusters. A structural feature is in that the six-metal $\{Na_2Cu_4\}$ central belt of anion contains the mixed valence states of Cu^{I}/Cu^{II} group. This compound shows excellent catalytic activity for effectively promoting inorganic electron transfer (redox) reaction of ferricyanide to ferrocyanide by thiosulphate with high rate constant value in aqueous solution. In addition, compound (**H_9-1**) also exhibits an inhibition effect for the organic photodegradation reaction of Rhodamine B (RhB).

1. Introduction

The synthesis and exploitation of polyoxometalates (POMs) have attracted considerable attention in recent years, owing to not only their diversities of shape, size, and redox properties but also their potential applications in catalysis, photochemistry, electrochemistry, and magnetism.[1-4] Although POMs has been known for about 200 years, the mechanism of formation of polyanionic clusters is not well understood and is commonly described as self-assembly. Therefore, systematic structural design for novel POMs and derivatization for known POMs are still an attractive and longstanding challenging topic. In material world, properties are determined by structures, so searching for new POM clusters with special active sites are ongoing.

Transition-metal substituted POMs (TMSPs) are well known, and numerous such complexes have been reported.[5] Among the class of TMSPs, the sandwich-type species represent a relatively larger subfamily.[6] As is well known, the Hervé-,[7] Krebs-,[8] Weakly-,[9] and Knoth-[10] sandwich-type polyoxoanions had been obtained and reported, and this kind of Sb^{III}-centered polyoxotungstates have been known for a long time.[11] Due to the existence of a lone pair of electrons on the heteroatom which precludes the formation of the most stable Keggin-type cluster, it is possible to obtain many more novel sandwich-type TMSPs with unprecedented structure and property. The Krebs group has reported a large number of heteropolyanions, such as $(C_{52}H_{60}NO_{12})_{12}[(Mn(H_2O))_3(SbW_9O_{32})_2]$, $[Mn^{II}_2(H_2O)_6(WO_2)\text{-}(SbW_9O_{32})_2]^{10-}$, $[M_2(H_2O)_6(WO_2)_2SbW_9O_{32})_2]^{10-}$ (M= Mn^{II}, Zn^{II}) and $[Sb_2W_{22}O_{74}(OH)_2]^{12-}$.[12-14] Their work indicated that the manganese(II)-contained polyoxoanion $[Mn^{II}_2(H_2O)_3(Sb\text{-}W_9O_{32})_2]^{12-}$ possesses highly efficient catalytic feature in the epoxidation of alkenes. The groups of Kortz and Proust respectively reported two compounds $(CsNa_2)[\{Sn(CH_3)\}_3\text{-}(H_2O)_4(\beta\text{-}SbW_9O_{33})]\cdot 7H_2O$ and $[Sb_2W_{20}O_{70}\{\rho\text{-cymene}\}_2]^{10-}$, being the first organotin derivative of $\beta\text{-}[SbW_9O_{33}]^{9-}$, and the first obtained organometallic heteropolytungstate related to $[Sb_2W_{22}O_{74}(OH)_2]^{12-}$ by self-assembly.[15-16] Very recently, Niu et al. reported the synthesis and magnetic property of five Sb^{III}-containing polyoxotungstates.[5] In 2012, our group reported on the synthesis of a $\{V{=}O\}_6$-containing inorganic-metal-organic sandwich-type tungstoantimonite in which was accompanied by *in situ* new carbon–carbon bond formation of organic cations.[17]

Atomic compositions and combination modes of the central belt have important influence on the physicochemical property of the last sandwich-type assemblies. Introduction of the active metal sites into polyanionic skeleton might adjust some parameters of physical property. In the current work, when Cu cations with the evident Jahn-Teller effect and flexible coordination geometries are utilized to hydrothermally react with Na_2WO_4, Sb_2O_3 and ethylenediamine(en), one distinctive inorganic sandwich-type tungstoantimonate $H_9[Na_2Cu^{I}Cu^{II}(OH_2)Cu^{II}_2(B\text{-}\alpha\text{-}SbW_9O_{33})_2]\cdot 9H_2O$ (**H_9-1**) has been successfully obtained and characterized. A structural feature is in that the six-metal central belt of anion contains mixed metal $\{Na_2Cu_4\}$ centers, and the copper atoms present mixed valence states of Cu^{I}/Cu^{II}. Its photodegradation behaviors for Rhodamine-B (RhB), as well the catalytic electron transfer(redox) for ferricyanide to ferrocyanide by thiosulphate have been investigated during our experiments. It is found that this compound shows excellent catalytic activity

for inorganic reduction reaction of ferricyanide to ferrocyanide by thiosulphate with high rate constant value in aqueous solution. But on the contrary, compound (**H_9-1**) exhibits an inhibition effect for the organic photodegradation reaction of RhB. A feature for POM catalyst is in their structural stability and integrality with nano-sized anionic cluster, which can be separated easily after reaction and reused.

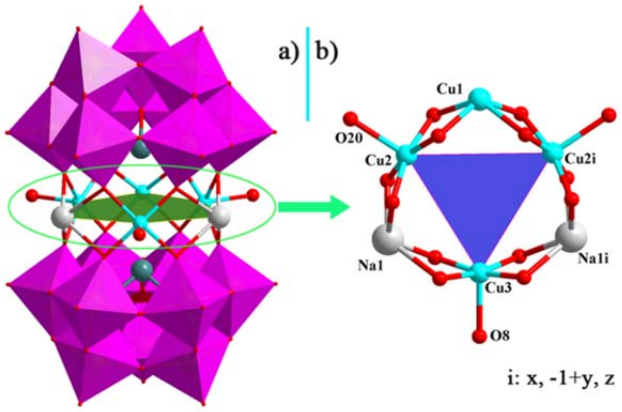

Figure 1. a) Polyhedral and ball-and-stick representation of the sandwich-type structural unit of **1**; b) Ball-and-stick representation of the central six-metal belt $\{Cu_4Na_2O_{15}\}$ in **1**. The $\{WO_6\}$ octahedra are shown in pink, and the balls represent Sb(teal), Na(gray), Cu(turquoise), O(red) atoms, respectively. Solvent water molecules are omitted for clarity.

2. Results and discussion

2.1. Structure description of compound (H_9-1)

Single-crystal X-ray diffraction study reveals that polyoxoanion in **1** consists of two $[B\text{-}\alpha\text{-}SbW_9O_{33}]^{9-}$ moieties with one mixed six-membered metal $\{Cu_4Na_2\}$ belt, resulting in the formation of sandwich-type cluster (see Figure 1a). The trivacant B-a-$[SbW_9O_{33}]^{9-}$ unit could be seen as a derivative from the parent α-Keggin structure by taking off three edge-sharing $\{WO_6\}$ octahedra. The $\{SbO_3\}$ tetrahedron located at the center is surrounded by three vertex-sharing $\{W_3O_{13}\}$ trimers. The central belt of polyanion is composed of three adjacent oxygen-shared copper ions (Cu(1), Cu(2) and Cu(2i)) and an isolated copper ion (Cu(3)) which is separated from the copper triad by two sodium ions, namely the six-membered center belt consists of one Cu^+(1), three Cu^{2+}(2/3) and two Na^+(1) ions within a plan (see Figure 1b). Interestingly, the central four copper ions are not completely equivalent each other because of their different coordinated environments, which could be grouped as three types: the first is two $\{Cu(2)O_5\}$ tetragonal pyramids, which are coordinated by four interior oxygen atoms from two $[\alpha\text{-}SbW_9O_{33}]^{9-}$ units and the vertex position is occupied by O_b shared with W atom (Cu(2)-O(20)-W(5)) from one adjacent polyanion; the second is $\{Cu(3)O_4(OH_2)\}$ with a similar polyhedral environment to Cu(2) except the vertex position occupied by one water molecule (Cu(3)-O(8) = 2.23(2) Å); the last type is that $\{Cu(1)O_4\}$ group is merely coordinated by four interior oxygen atoms from two $[\alpha\text{-}SbW_9O_{33}]^{9-}$ subunits.

As shown in our previous work[17] on six-metal cations in sandwich-type POMs, **1** represents a new member in this family. It is of interest to discuss their bond lengths and angles within the central mixed-metal section of polyanion. The three five-coordinated Cu^{2+} ions are arranged in an approximately equilateral triangle with distances of Cu(2)…Cu(3) = 4.8175(37) Å, Cu(2)…Cu(2i) = 4.8608(23) Å and angles of Cu…Cu…Cu = 59.70º and 60.60° (see Figure 1b), respectively. Moreover, the square-pyramidal coordination spheres of Cu(2) (Cu(2)–Oeq = 1.933(9) Å; Cu(2)–Oax = 2.263(13) Å) and Cu(3) (Cu(3)–Oeq = 1.937(10) Å; Cu(3)–Oax = 2.23(2) Å) are fairly regular and exhibit the expected Jahn–Teller distortion (axial elongation). However, the Cu(1)(Cu(1)–Oeq = 2.149(9) Å) located between two Cu(2) atoms exhibits a distorted square-planar coordination. In addition to the four copper ions, the central belt of polyanion **1** also incorporates two Na^+ ions which are located in two sides of equilateral triangle of copper ions, and are bond to four oxygen atoms from two $\{SbW_9O_{33}\}$ fragments with the expected bond lengths ranges (Na(1)…O = 2.161(12)–2.352(14) Å). To the best of our knowledge, a structure[5] of previously reported $[Na_2Cu_4Cl(B\text{-}a\text{-}SbW_9O_{33})_2]^{9-}$ is similar to that in **1**, but mainly arising from the highly disordered positions of Cu and Na sites, respectively.

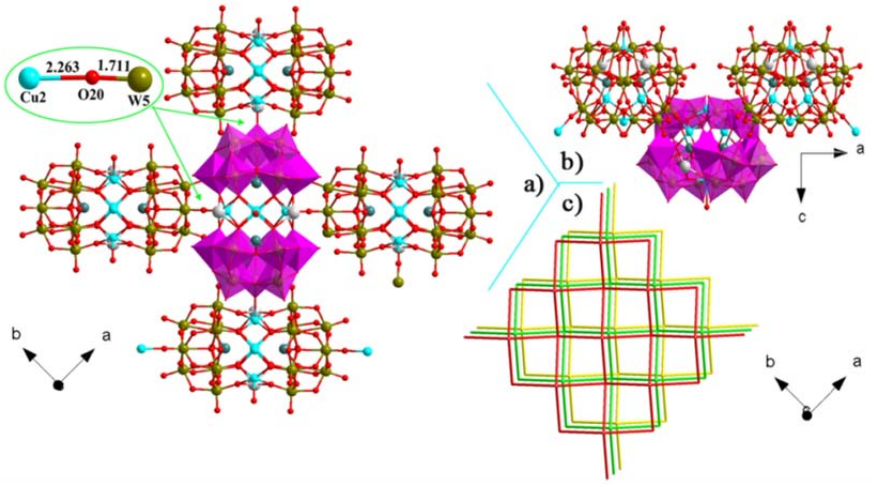

Figure 2. a) polyhedral/ball-and-stick representation showing the connectivity sheet of neighbouring polyanions by Cu(2)-O(20)-W(5) bridges in the lattice of **1**; b) a side view of sheet seen along *b* axis; c) a simplified stacking scheme showing the arrangement of different inorganic sheets, each node represents that of anion **1**. The color codes are the same as that in Figure 1.

Journal Name RSCPublishing

ARTICLE

Furthermore, the results of bond valence calculations[18] for **1** show +1 for Cu(1), +2 for Cu(2/3) and +6 for W centers, respectively, which have also been confirmed by XPS measures. These oxidation states of atoms are good consistent with their coordination environments. It should be noted that this kind of Cu^{I}/Cu^{II} mixed oxidation state should be ascribed to the reduction activity of organic amine during hydrothermal reaction. So en here plays double roles of structure-template and reducing agent during the reaction.

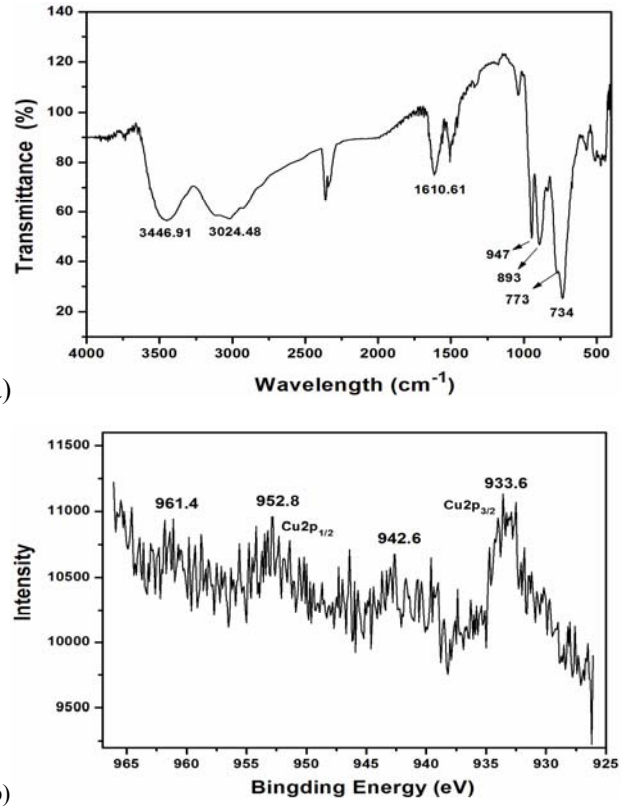

a)

b)

Figure 3. a) IR Spectroscopy; b) XPS of Cu in compound **1**.

The 2D structure of (**H_9-1**) is composed of individual polyoxoanions connected to four neighbors via four Cu(2)–O(20)–W(5) bridges. The two equivalent copper centers Cu(2) and Cu(2i) share the terminal oxygen donors with tungsten centers W(5) of the two adjacent polyanions. Simultaneously, the two symmetrically equivalent tungsten centers W(5) and W(5i) in **1** are linked to the two equivalent copper atoms Cu(2) from the two adjacent polyanions (see Figure 2a). This solid-state structure distribution is a clear result of the unsymmetrical composition of four copper ions within the central ring of each polyanion **1**. Three of the four copper ions (Cu(2), Cu(2i), Cu(1)) are close on the "copper-rich" side of the ring, whereas the Cu(3) is located on the "copper-poor" side of the ring (separated from each other by the two equivalent sodium ions Na(1) and Na(1i)) (see Figure 1b). The lattice of (**H_9-1**) can be described as double layers of **1** where the copper-rich sections of the central belt point at each other (see Figure 2b). Polyanions in one layer are arranged vertically each other, whereas the other layer are arranged horizontally, and all polyanions in the "vertical layer" are completely parallel, leading to a charming 2D (4,4') network (see Figure 2c). As we know, the extended 2D-netlike-structure based on sandwich type tungstoantimonate containing mixed valence copper ions in the central belt has not been reported.

2.2. IR spectroscopy and XPS of Cu in H_9-1

In IR spectrum of compound (**H_9-1**), the peaks at 947, 893, 773 and 734 cm^{-1} are attributed to the characteristic vibrations of ν(Sb-O_a), ν(W-O_d), ν(W-O_b-W) and ν(W-O_c-W), respectively. The strong peak at 1610 cm^{-1} is assigned to ν(H-O-H). In addition, the wide bands between 2800 and 3450 can be assigned to ν(O-H) (see Figure 3a).[14] The existence of Cu^{I} and Cu^{II} in the (**H_9-1**) is confirmed by XPS measurement (see Figure 3b). The XPS spectrum of the pure sample displays the peaks of $Cu2P_{3/2}$ and $Cu2P_{1/2}$ at 933.6 and 952.8 eV attributable to Cu^{I}, and the peaks at 942.6 and 961.4 eV indicate the presence of Cu^{II} ion.[19] XPS spectra also confirm the existence of W^{VI} and Sb^{III} in **1** (Figs. S1 and S2).

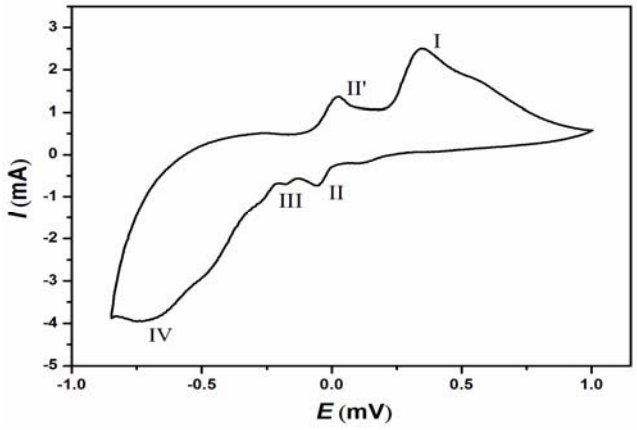

Figure 4. Cyclic voltammogram of the **1**-CPE in the 1 mol·L^{-1} H_2SO_4 solution, scan rate: 5 mV·s^{-1}, *vs.* SCE.

2.3. Voltammetric behaviour

To study the redox property of compound (**H_9-1**), **1**-modified CPE (**1**-CPE) was fabricated as the working electrode, according to the method described in Section 2. The cyclic voltammetric behavior of **1**-CPE in 1 mol·L^{-1} H_2SO_4 solution in the range from +1.00 V to – 0.85 V at a scan rate of 5 mV·s^{-1} is displayed in Figure 4. In the potential domain explored, it consists of three obvious reduction waves with peak potentials located at -0.055 V (II), -0.170 V (III) and -0.704 V (IV) vs SCE, respectively. In the voltammogram, the first oxidation peak (I) for **1**-CPE is attributed to oxidation processes of the $Cu^0 \rightarrow Cu^{2+}$, and the second pair of quasi-reversible redox peaks (II-II') is attributed to the redox process of the $Cu^+ \rightarrow$

Cu^{2+}.[20-21] While, the last two waves (III and IV) for **1**-CPE are assigned to the redox processes of W atoms in the polyoxoanion framework, and the domain where the waves are located, was also observed in the other tungsten-containing POMs.[22-24]

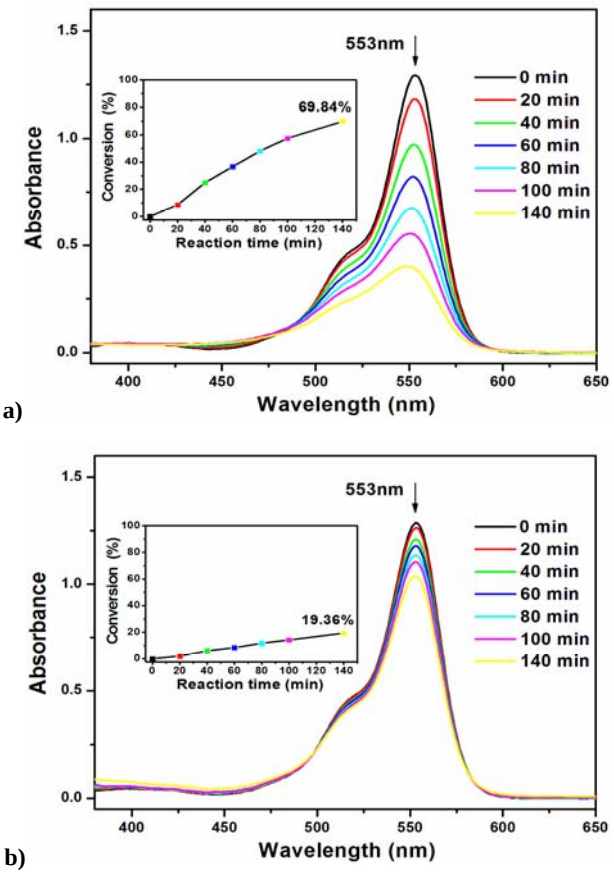

Figure 5. a) UV-visible absorption spectra of RhB solutions at various UV irradiation times as a blank experiment; b) UV-visible absorption spectra of RhB solutions at various UV irradiation times with the existence of compound (**H_9-1**). Insets: the conversion of RhB (K) with reaction time (*t*).

2.4. Catalytic study

2.4.1 Photocatalysis

POM-based photocatalytically active materials have received much attention, because a variety of organic substrates can be oxidized photocatalytically, even mineralized, by POMs under UV-visible irradiation.[25-27] In this experiment, we examined the degradation process of RhB by 500W Hg lamp irradiation in the presence of (**H_9-1**) as photocatalyst. As is well-known, the RhB substrate consisting of four N-ethyl groups at either side of the xanthene ring is relatively stable in aqueous solution in darkness or upon visible light irradiation.[25] When RhB solution is kept in darkness either in the presence of or in the absence of (**H_9-1**), the degradation reactions of RhB hardly happened (Figs. S3 and S4). It can also be found that crystals do not have obvious adsorption performance for RhB. However, the RhB substrate in the absence of (**H_9-1**) undergoes pronounced photodegradation in aqueous solution upon 500W Hg lamp irradiation, and the UV-visible spectral maximum absorbance of the degradation solution decreases from 1.71 to 0.54 after 140 min (see Figure 5a). The UV-visible spectral change processes during the photodegradation of RhB at various times in the presence of (**H_9-1**) is shown in Figure 5b. Interestingly, compared with that in the absence of (**H_9-1**), the UV-visible spectral maximum absorbance of the degradation solution in the presence of (**H_9-1**) slowly decreases from 1.71 to 1.36, after 140 min, proving that (**H_9-1**) can to some extent inhibit the photodegradation of RhB. The phenomenon is different from those POM-based compounds that can promote the photodegradation of RhB.[25-26] The characteristic absorption peaks of RhB (around 553 nm) are chosen to study the conversion of RhB. The plots of the conversion of RhB (K) varying with reaction time (*t*) are shown in the insets of Figure 5. The conversion of K can be expressed as $K = (I_0 - I_t)/I_0$, where I_0 represents the UV-visible absorption intensity of RhB at the initial time ($t = 0$) and I_t is the UV-visible absorption intensity at a given time (*t*).[28] The conversion of RhB in the absence of (**H_9-1**) upon irradiation for 140 min is *ca*. 69.84%, while the conversion of RhB in presence of (**H_9-1**) is only 19.36%, which also reveals the inhibiting effect for RhB. the main reasons might be as follows: (i) **1** can work as absorbers of the Hg lamp irradiation; (ii) it is found in experiments that the crystal of **1** is only sparingly soluble, resulting that a very small amount of polyanions dissolve in solution. The hydrogen-bonding interactions between donors of RhB substrates ($N(C_2H_5)_2$, COOH) and acceptors of (**H_9-1**) (surface oxygen atoms of POMs) enhance the chemical stability of RhB substrate in solution, which leads to the slow photodegradation of RhB substrates.[2] In addition, IR spectrum of (**H_9-1**) after the photocatalytic degradations was also measured, which proves that the structure of (**H_9-1**) is still retained after the photocatalytic experiment (Fig. S5). The recycle experiments show that compound (**H_9-1**) maintained high inhibition performance after 2 repeated experiments (Figs. S6 and S7). Obviously, the inhibiting the photodegradation experiment of RhB is interesting to explore many functionalized TMSP compounds as color protection agent.

2.4.2 Catalytic Studies for Reduction of $Fe(CN)_6^{3-}$ by $S_2O_3^{2-}$

The catalytic electron transfer property of compound (**H_9-1**) is tested in case of the inorganic redox reaction between $Fe(CN)_6^{3-}$ and $S_2O_3^{2-}$ at room temperature (25°C) and 55°C, respectively. This reaction could hardly occur in absence of catalyst at that temperatures.[29] It has been recently reported that the noble Au or Pt nanoparticals (NPs) are much more catalytically active for this redox reaction.[30-32] However, the rate of reaction was slow at 25 ºC as observed by other workers using Au and Pt NPs as catalysts. Earlier work also confirmed that the catalysis reaction occurred through the electron transfer at the noble metal Au or Pt surface. Sandwich-type polyanion (**H_9-1**) as a nano-sized cluster has a large metal delocalized π bond located at the surface, which might be more conducive to electron transfer. The reduction process is monitored with respect to time using UV-visible spectrometer. The depletion of $Fe(CN)_6^{3-}$ peak at 420 nm has been used to study the rate of such catalyzed reaction. Fortunately, the experimental result reveals that the (**H_9-1**) is catalytically active for this inorganic redox reaction. We found that the electron transfer reaction proceeds difficultly using compound (**H_9-1**) as catalyst at room temperature (Figure 6a). However, the rate of reaction and reduction degree increases a lot at higher temperature (55 ºC) (Figure 6b). The apparent rate constant values calculated from the slope of the plot of $-\ln A_{420}$ against time are $k = 1.23 \times 10^{-3}$ min^{-1} at 25 ºC and $k = 9.52 \times 10^{-3}$ min^{-1} at 55 ºC, respectively (Figure 6c). The *k* parameter is even higher than that was observed in the presence of Au doped mesoporous boehmite film material as catalyst (the $k = 8.43 \times 10^{-3}$ min^{-1} at 55 ºC).[29]

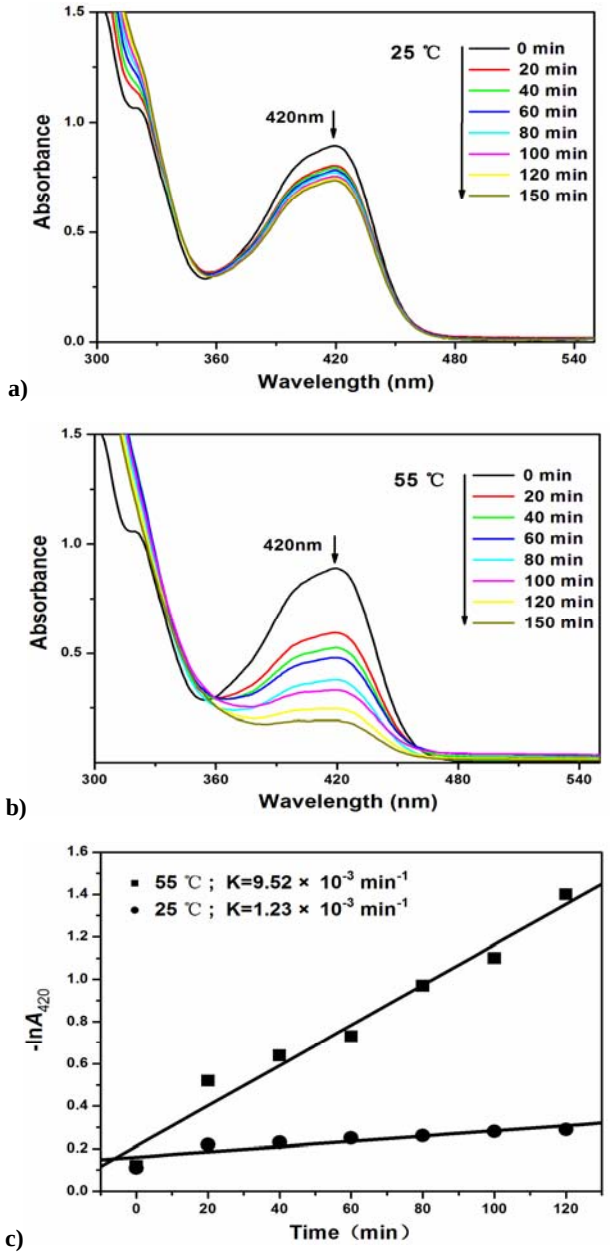

Figure 6. Successive UV-visible absorption spectra of the reduction of $Fe(CN)_6^{3-}$ in the presence of (**H_9-1**) at two different temperatures: a) 25ºC; b) 55ºC; c) the pseudo first order plots of –ln *A* (absorbance intensity at 420 nm) versus time for the above reactions.

With the consideration of compound (**H_9-1**) may be partially dissolved in this case, by contrast, the simple catalytic redox comparative experiments were also completed in the similar fashion with the use of WO_3 (abbreviated as W), Sb_2O_3+WO_3 (abbreviated as Sb+W), CuO+WO_3 (abbreviated as Cu+W) and CuO+Sb_2O_3+WO_3 (abbreviated as Cu+Sb+W), respectively. The ratio of metal oxides is calculated according to the corresponding value in **1**. As illustrated in Figure 7, changes in the concentration of $Fe(CN)_6^{3-}$ solution are versus reaction time. It can be seen that the catalytic activity increases from 10% for Sb+W, 24% for W, 35% for Cu+Sb+W and 39% for Cu+W to 78% for compound (**H_9-1**) after 2.5 h of reaction time. With a rate of 1.664 mg L^{-1} min^{-1} for the reduction of $Fe(CN)_6^{3-}$ solution catalyzed by (**H_9-1**), approximately 50% of $Fe(CN)_6^{3-}$ had been reduced within an hour, which indicates that the probable synergistic effect between the transition metals assembled in polyanionic cluster produce a higher catalytic activity of compound (**H_9-1**) for the reduction of $Fe(CN)_6^{3-}$. In addition, when compared mixed metal oxides with WO_3 alone, it is easy to find that the presence of Sb_2O_3 and CuO may play a role in inhibiting and promoting respectively for the reduction reaction of $Fe(CN)_6^{3-}$. Through these results above-mentioned, it can also be concluded that compound (**H_9-1**) does not decompose but just partially dissolve in the solution during the reaction process, which is probably affected by high temperature. In contrast to the previously reported using precious metal Au and Pt NPs as catalysts, compound (**H_9-1**) is cheaper and easier to synthesize. Furthermore, the repeated experiment had also been done, but the result displayed that the catalytic performance of (**H_9-1**) declined a lot (Fig. S8). A possible reason is that the surface of (**H_9-1**) adsorbs a lot of $Fe(CN)_6^{4-}$, which could impede the contact (**H_9-1**) and $Fe(CN)_6^{3-}$, reducing the catalytic activity. The IR spectrum of (**H_9-1**) after the catalytic reduction may be used to prove it (Fig. S9). Much work needs to done for addressing more problems.

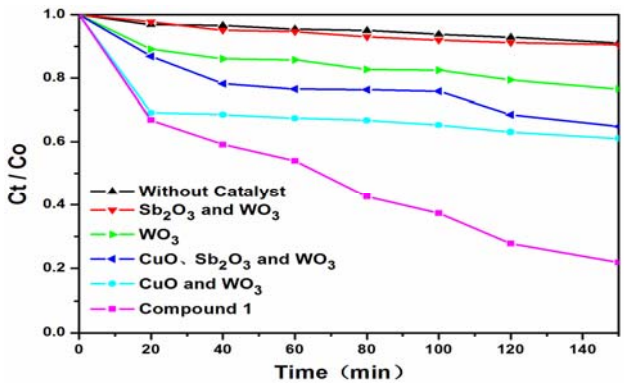

Figure 7. UV-visible absorption spectra of the reduction of $Fe(CN)_6^{3-}$ with the use of five groups of catalysts, and black curve is the control experiment without any catalyst. (The ratio of metal oxides is calculated according to the corresponding value in **1**; the reaction temperature is at 55 °C).

3. Experimental section

3.1. Synthesis and characterization

All chemicals are commercially purchased and used without further purification. FTIR spectrum is recorded in a KBr pellet with a FTIR-8900 IR spectrometer in the range of 400-4000 cm^{-1} region. Thermogravimetric analysis (TG) is carried out using a Perkin-Elmer Pyris Diamond TG/DTA instrument in flowing N_2 with a heating rate of 10°C/min. Powder X-ray diffraction (XRD) is determined by a Bruker AXS D8 Advance diffractometer. Cyclic voltammogram (CV) is obtained with a CHI 660B electrochemical workstation at room temperature. UV spectra are measured by U3010 UV–visible spectrophotometer (Shimadzu).

3.1.1 Synthesis of compound (H_9-1)

A mixture of $Na_2WO_4{\cdot}2H_2O$ (400 mg, 1.2 mmol), Sb_2O_3 (50 mg, 0.17 mmol), $Cu(CH_3COO)_2{\cdot}H_2O$ (0.25mg, 1.2 mmol), en (0.4 mL, 5.92 mmol) was dissolved in 10 mL distilled water at room temperature. The pH value of the mixture was adjusted to

ca. 3.7 with 4 mol·L^{-1} HCl. Then the suspension was put into a Teflon-lined autoclave and kept under autogenous pressure at 180 ºC for 5 days. After slow cooling to room temperature at a rate of 10 ºC·h^{-1}, green tetragonal crystals were filtered and washed with distilled water (35% yield based on W).

The XRD and TG curves for compound (**H_9-1**) were provided into Supporting materials as Figs. S10, S11, respectively.

3.2. X-ray crystallography

Single crystal of compound (**H_9-1**) was selected for data collection performed on a Smart Apex CCD diffractometer diffractometer at 296(2) K with MoKα monochromated radiation (λ= 0.71073 Å). The structure was solved by direct methods and refined by the full-matrix least-squares method on F^2 using the SHELXTL-97 program package.[33] Anisotropic thermal parameters were used to refine all non hydrogen atoms. The limiting indices were (−17≤ h ≤19, −15≤ k ≤19, −16≤ l ≤15) for (**H_9-1**). CCDC-1017979 contains the crystallographic data for the paper. All crystal data and structure refinement details for the compound (**H_9-1**) were given in Table 1.

Table 1 Crystal data and structure refinement details for the compound (**H_9-1**)

Empirical formula	$Cu_4H_{23}Na_2O_{76}Sb_2W_{18}$
Formula weight	5068.94
Crystal system	Tetragonal
Space group	*P*-42(1)*m*
a, *b*, *c* /Å	16.466(4),16.466(4), 14.115(6)
α, β, γ /°	90
Volume /Å^3, *Z*	3827(2), 2
Density (calculated) /(Mg/m^3)	4.399
Absorption coefficient	28.820
$F_{(000)}$	4360
Crystal size / mm^3	0.17 × 0.15 × 0.13
Theta range	1.90-25.01°
Reflections collected	18926
Independent reflections /$R_{(int)}$	3552 (0.0393)
Completeness	99.6
Absorption correction (%)	Empirical
Max. and min. transmission	0.024 and 0.010
Data / restraints / parameters	3552 / 0 / 259
Goodness-of-fit on F^2	1.045
Final *R* indices [*I*>2sigma(*I*)]	R_1 = 0.0265, wR_2 = 0.0651
R indices (all data)	R_1 = 0.0302,wR_2 = 0.0674

3.3. Methods and materials

3.3.1 Electrochemical property

Cyclic voltammetry measurements were carried out on a CHI 660 electrochemical workstation at room temperature. Platinum gauze was used as a counter electrode and a saturated calomel electrode (SCE) was used as reference electrode. Chemically bulk-modified carbon paste electrodes (CPEs) were used as the working electrodes.

The compound (**H_9-1**) modified CPEs (**1**-CPE) was fabricated as follows: 0.1 g of graphite powder and 0.01 g of (**H_9-1**) were mixed and ground together by an agate mortar and pestle to achieve a uniform mixture, and then was added 0.1 mL paraffin oil with stirring. The homogenized mixture was packed into a plastic tube with 2 mm inner diameter. Electrical contact was established with a copper rod through the back of electrode.

3.3.2 Photocatalytic reaction

Photocatalytic reactions were carried out in a light reaction tube of 50 mL capacity attached to an inner radiation type. 25 mg crystal (**H_9-1**) was dispersed into aqueous solution containing RhB (10 mg·L^{-1}). Then the mixture was stirred continuously under ultraviolet (UV) irradiation from a 500W high pressure mercury vapour lamp. A sample was taken every 20 min and then centrifuged to remove the particles of catalyst, but the starting point did not contain the first 10 min in order to rule out the effect of its absorption to the particle surfaces. Changes in the value of the maximum absorbance at 553 nm were used to measure the degradation rate of RhB.

3.3.2 Catalytic reduction of $Fe(CN)_6^{3-}$

In this experiment, 35 mg compound (**H_9-1**) was mixed together with 16 mg $K_3Fe(CN)_6$ and 108 mg $Na_2S_2O_3{\cdot}5H_2O$ dissolving in 50 mL distilled water at 55 °C. Then the mixture was stirred continuously. Every 20 min interval, 5mL aliquot was sampled and then centrifuged to remove the particles of catalyst. The $Fe(CN)_6^{3-}$ concentration (*C*) was determined by measuring the maximum absorbance at 420 nm as a function of irradiation time using a U3010 UV–visible spectrophotometer (Shimadzu). The amount of catalysts in the reference tests were calculated according to the corresponding metal oxides mass fraction in compound (**H_9-1**).

4. Conclusions

In summary, a novel sandwich-type transition-metal-substituted tungstoantimonate has been hydrothermally synthesized and structurally characterized. The sandwich-type skeleton $[Na_2Cu^ICu^{II}(OH_2)Cu^{II}_2(B\text{-}\alpha\text{-}SbW_9O_{33})_2]^{9-}$ is composed of two trivacant Keggin $[B\text{-}\alpha\text{-}SbW_9O_{33}]^{9-}$ moieties linked by a belt six-membered ring cluster $\{Na_2Cu_4\}$ displaying an intriguing 2D-netlike structure in a paralleled fashion. Voltammetric behavior of (**H_9-1**) has been investigated. Furthermore, the catalytic activity of (**H_9-1**) for the photocatalytic degradation of RhB and the reduction of ferricyanide to ferrocyanide by thiosulphate has been explored. Especially, in contrast to the previously reported using precious metal Au and Pt NPs as catalysts for electron transfer reaction, compound (**H_9-1**) is cheaper and does better. This work provides a new idea for POM-based materials' application. Currently, we are trying to synthesize many more different sandwich type transition-metal substituted POMs with novel structure and special features.

Acknowledgments

This work was financially supported by the Natural Science Foundation of China (21341003, 21272054), and the Hebei Natural Science Foundation of China (No. B2011205035).

Notes and references

[a] College of Chemistry and Material Science, Hebei Normal University, No. 20 Road East of 2nd Ring South, Yuhua District, Shijiazhuang, Hebei 050024, China.

† Electronic Supplementary Information (ESI) available: the additional XPS, UV, IR, XRD, and TG curves, See DOI: 10.1039/b000000x/

1 D. L. Long, R. Tsunashima and L. Cronin, *Angew. Chem., Int. Ed.,* 2010, **49**, 1736.
2 Z. G. Han, X. Q. Chang, J. S. Yan, K. N. Gong, C. Zhao and X. L. Zhai, *Inorg. Chem.,* 2014, **53**, 670-672.

3 H. C. Li, X. Yu, H. W. Zheng, Y. M. Li, X. H. Wang and M. X. Huo, *RSC Adv.,* 2014, **4**, 7266-7274.
4 D. M. Fernandes, L. C. Silva, R. A. S. Ferreira, S. S. Balula, L. D. Carlos, B. D. Castro and C. Freire, *RSC Adv.,* 2013, **3**, 16697.
5 J. P. Wang, P. T. Ma, J. Li, H. Y. Niu and J. Y. Niu, *Chem. Asian. J.,* 2008, **3**, 822.
6 M. T. Pope, *Comp. Coord. Chem. II.,* 2003, **4**, 635.
7 U. Kortz, S. Isber, M. H. Dickman and D. Ravot, *Inorg. Chem.,* 2000, **39**, 2915.
8 B. Botar, T. Yamase and E. Ishikawa, *Inorg. Chem. Commun.,* 2001, **4**, 551.
9 D. Drewes, E. M. Limanski, M. Piepnbink and B. Krebs, *Z. Anorg. Allg. Chem.,* 2004, **630**, 58.
10 F. B. Xin and M. T. Pope, *J. Am. Chem. Soc.,* 1996, **118**, 7731.
11 J. Fischer, L. Richard and R. Weiss, *J. Am. Chem. Soc.,* 1976, **98**, 3050.
12 D. Volkmer, B. Bredenkötter, J. Tellenbröker, P. Kögerler, D. G. Kurth, P. Lehmann, H. Schnablegger, D. Schwahn, M. Piepenbrink and B. Krebs, *J. Am. Chem. Soc.,* 2002, **124**, 10489.
13 M. Piepenbrink, E. M. Limanskiu and B. Krebs, *Z. Anorg. Allg. Chem.,* 2002, **628**, 1187.
14 M. Bösing, I. Loose, H. Pohlmann and B. Krebs, *Chem. Eur. J.,* 1997, **3**, 1232.
15 F. Hussain, M. Reicke and U. Kortz, *Eur. J. Inorg. Chem.,* 2004, **13**, 2733.
16 D. Laurencin, R. Villanneau, P. Herson, R. Thouvenot, Y. Jeannin and A. Proust, *Chem. Commun.,* 2005, **44**, 5524.
17 Z. G. Han, Q. X. Zhang, Y. Z. Gao, J. J. Wu and X. L. Zhai, *Dalton Trans.,* 2012, **41**, 1332-1337.
18 I. D. Brown and D. Altermatt, *Acta Cryst. B,* 1985, **41**, 244-247.
19 L. M. Zheng, P. Yin, X. Q. Xin, *Inorg. Chem.,* 2002, **41**, 4084-4086.
20 B. Keita, E. Abdeljalil, L, Nadjo, R. Contant and R. Belgiche, *Electrochem. Commun.,* 2001, **3**, 56.
21 A. X. Tian, J. Ying, J. Peng and J. Q. Sha, *Inorg. Chem.,* 2008, **47**, 3274.
22 B. S. Bassil, U. Kortz, A. S. Tigan, J. M. Clemente-Juan, B. Keita, P. Oliveira and L. Nadjo, *Inorg. Chem.,* 2005, **44**, 9360.
23 B. S. Bassil, S. Nellutla, U.Kortz, A. C. Stowe, J. van Tol, N. S. Dalal, B. Keuta and L. Nadjo, *Inorg. Chem.,* 2005, **44**, 2659-2665.
24 I. M. Mbomekalle, B. Keita, M. Nierlich, U. Kortz, P. Berthet and L. Nadjo, *Inorg. Chem.,* 2003, **42**, 5143-5152.
25 C. C. Chen, W. Zhao, P. O. Lei, J. C.Zhao and N. Serpone, *Chem. Eur. J.,* 2004, **10**, 1956.
26 Q. Wu, W. L. Chen, D. Liu, C. Liang, Y. G. Li, S. W. Lin and E. B. Wang, *Dalton Trans.,* 2011, **1**, 56.
27 I. A. Weinstock, *Chem. Rev.,* 1998, **98**, 113.
28 J. W. Zhao, D. Y. Shi, L. J. Chen, X. M. Cai, Z. Q. Wang, P. T. Ma, J. P. Wang and J. Y. Niu, *CrystEngComm.,* 2012, **14**, 2797.
29 D. Jana, A. Dandapat and G. De, *Langmuir.,* 2010, **26**, 12177.
30 K. H. Su, Q. H. Wei, X. Zhang, J. J. Mock, D. R. Smith and S. Schultz, *Nano Letters.,* 2003, **3**, 1087.
31 S. K. Medda, S. De and G. J. De, *Mater. Chem.*, 2005, **15**, 3278.
32 A. Pöppl, T. Rudolf and D. Michel, *J. Am. Chem. Soc.,* 1998, **120**, 4879.
33 G. M. Sheldrick, SHELXTL-97, Programs *for Crystal Structure Refinement*, University of Göttingen, Germany, 1997.